OPTIMAL GRIDS FOR ANISOTROPIC PROBLEMS[*]

S. ASVADUROV[†], V. DRUSKIN[‡], AND S. MOSKOW[§]

Abstract. Spectral convergence of optimal grids for anisotropic problems is both numerically observed and explained. For elliptic problems, the gridding algorithm is reduced to a Stieltjes rational approximation on an interval of a line in the complex plane instead of the real axis as in the isotropic case. We show rigorously why this occurs for a semi-infinite and bounded interval. We then extend the gridding algorithm to hyperbolic problems on bounded domains. For the propagative modes, the problem is reduced to a rational approximation on an interval of the negative real semiaxis, similarly to in the isotropic case. For the wave problem we present numerical examples in 2-D anisotropic media.

Key words. finite differences, DtN maps, anisotropy, spectral approximation

AMS subject classifications. 65M06, 65N06

1. Introduction. The Dirichlet-to-Neumann (DtN) operator is an important tool for many applications, such as inverse problems [19], domain decomposition [1, 18, 12], and absorbing boundary conditions [11, 13, 15]. So, it sounds attractive to target computational algorithms to generate accurate approximations of the DtN map at the expense of accuracy in the entire domain. The use of specially placed finite difference grid points have proven useful for several problems in geophysics described by isotropic PDEs. These grids are generated from rational approximations of the DtN map, or impedance function in the spectral domain. See, for example [8] for an introduction and their generation algorithm; [3, 4, 2, 6] for their application to geophysical problems and inversion; and [10] for their relationship with spectral methods. The staggered finite difference grids are chosen to yield exponential convergence for the model problem

$$(1.1) \qquad \lambda u - u_{xx} = 0$$

at the endpoint receiver location(s) for λ in a given spectral interval. The grids are then applied to more complex problems, such as higher dimensional (isotropic) wave propagation, and the observed spectral convergence at receivers can be explained by Fourier transform reduction of the problem to (1.1). Furthermore, since the DtN map completely describes the coupling of a domain with its neighbors, these grids can be combined with domain decomposition to yield spectral convergence in piecewise constant media with Cartesian interfaces [3, 9].

In geophysics, however, one frequently deals with piecewise smooth media which are inherently anisotropic, or that involve layers dipped at various angles. For example, we may be interested in two dimensional scalar wave propagation in such media, modelled piecewise by

$$(1.2) \qquad u_{tt} = u_{xx} + 2au_{xy} + u_{yy}.$$

At first glance it is not obvious how to even apply the optimal grids to such a problem. On staggered grids, the mixed derivative term would require us to sum terms which live on

[†] McKinsey and Company, Inc., Russia, Moscow, Russia 115054, Paveletskaya square 2/2 (asvaduro@gmail.com).

[‡] Schlumberger Doll Research 320 Bent St., Cambridge, MA 02141-2025 (druskin1@boston.oilfield.slb.com).

[§] Department Of Mathematics, University of Florida 358 Little Hall, P.O. Box 118105 Gainesville, FL 32611-8105 (moskow@math.ufl.edu).

different grids. To resolve this issue on unbounded intervals, we use Lebedev grid clusters [16, 17, 7], which generally lead to natural extensions to anisotropy. For bounded problems, we split the solution into its odd and even parts. We describe the techniques in more detail throughout the paper.

Using the Lebedev cluster technique, when the above mentioned optimal grids were applied to (1.2), spectral convergence was observed at the receivers, despite the fact that the equation does not transform into (1.1). Indeed, even the steady state counterpart to (1.2),

$$u_{xx} + 2au_{xy} + u_{yy} = 0$$

becomes

$$(1.3) \qquad \lambda u - i2a\sqrt{\lambda}u_x - u_{xx} = 0$$

after Fourier transform in the y direction. Our goal is to explain why, then, the spectral convergence still occurs. To do this, we:

- explore rigorously in one dimension the use of grids which were optimized for (1.1) on the problem (1.3).
- explain how the convergence for (1.2) depends on the convergence of these grids for the problem (1.3).

The paper is organized as follows. In Section 2 we provide background on optimal grids, including a basic introduction in 2.1 and a demonstration of how they work for isotropic elliptic and wave problems in 2.2 and 2.3. Section 3 contains the study of anisotropy. In 3.1 we motivate our 1-d model with an elliptic equation. In 3.2 we show how to apply optimal grids to the anisotropic problem (1.3) on a half-line and prove that exponential convergence is maintained. We handle a slightly more general problem in a bounded interval in 3.3. In 3.4 and 3.5 we apply these results for a bounded interval to an anisotropic elliptic and wave problem, respectively. We present numerical experiments in Section 4 and a discussion in Section 5.

2. Background.

2.1. Optimal grids.
We first describe the optimal grid technique for background and notation. Consider the isotropic one dimensional problem on an interval $(0, L)$:

$$(2.1) \qquad \begin{aligned} \lambda u - u_{xx} &= 0 \\ -u_x(0) &= \alpha \\ u(L) &= 0 \end{aligned}$$

where our goal is to approximate the solution at the left endpoint, $u(0)$. (Source and receiver are at $x = 0$.) We note that we allow the case $L = \infty$. We use a staggered three-point finite difference scheme. Staggered schemes have primary and dual grids:

$$\{x_i\}, \quad i = 1, 2, \ldots, k + 1, \quad x_1 = 0$$

and

$$\{\hat{x}_i\}, \quad i = 0, \ldots, k, \quad \hat{x}_0 = 0,$$

respectively, with corresponding step sizes

$$h_i = x_{i+1} - x_i$$

$$\hat{h}_i = \hat{x}_i - \hat{x}_{i-1}.$$

One thinks of the potential u as living on the primary grid and the derivative u_x as living on the dual grid. Differences are three-point; taking them shifts a discrete solution from one grid to the other. The grid is staggered in the sense that the dual points are placed between two primal points, with the exception of the left endpoint which both grids share. We apply the Neumann boundary condition at $x = 0$ by using a ghost point to obtain the system for an approximation U to the solution to (2.1)

$$(2.2) \qquad \frac{1}{\hat{h}_i}\left(\frac{U_{i+1} - U_i}{h_i} - \frac{U_i - U_{i-1}}{h_{i-1}}\right) - \lambda U_i = 0 \quad i = 2, \ldots, k$$

$$\frac{1}{\hat{h}_1}\left(\frac{U_2 - U_1}{h_1}\right) - \lambda U_1 = -\frac{\alpha}{\hat{h}_1}$$

$$U_{k+1} = 0.$$

The second equation of (2.2) results from allowing $i = 1$ in the first equation of (2.2), and setting

$$\frac{U_1 - U_0}{h_0} = -\alpha,$$

where U_0 is the fictitious value at the ghost point x_0. Or, we may also use the notation

$$(2.3) \qquad (dU)_i = \frac{U_{i+1} - U_i}{h_i} \quad i = 0, 1, \ldots k,$$

and

$$(2.4) \qquad \left(\hat{d}\hat{U}\right)_i = \frac{\hat{U}_i - \hat{U}_{i-1}}{\hat{h}_i} \quad i = 1, 2, \ldots, k$$

for the difference operators from the primary to dual grid and from the dual to primary grid, respectively. We then can express the above difference equation as

$$\hat{d}dU - \lambda U = 0$$

$$-(dU)_0 = \alpha$$

$$U_{k+1} = 0.$$

For shorthand we will write the system in matrix notation:

$$(2.5) \qquad (L_h - \lambda)U = -\frac{\alpha}{\hat{h}_1}\vec{e}_1.$$

The continuous Neumann to Dirichlet, or NtD, map is the mapping $f(\lambda)$ from the Neumann data α to the Dirichlet data $u(0)$, with parameter λ:

$$u(0) = -f(\lambda)u'(0).$$

One can compute f explicitly; for finite L,

$$(2.6) \qquad f(\lambda) = \frac{\tanh\left(L\sqrt{\lambda}\right)}{\sqrt{\lambda}}$$

and for $L = \infty$

$$(2.7) \qquad\qquad f(\lambda) = 1/\sqrt{\lambda}.$$

Similarly, we can talk about the discrete NtD map, $f_k(\lambda)$ which is grid-dependent:

$$(2.8) \qquad\qquad U_1 = -f_k(\lambda)\frac{U_1 - U_0}{h_0}.$$

With a bit of algebra we can see that this discrete NtD map, or finite difference impedance, can be written as the rational function of λ

$$(2.9) \qquad\qquad f_k(\lambda) = \sum_{i=1}^{k} \frac{y_i}{\lambda - \theta_i}$$

where the $\theta_i < 0$ are the eigenvalues of L_h in (2.5) and $y_i > 0$ are the squares of the first components of the corresponding eigenvectors (normalized with respect to an $\hat{h}_i$ weighted inner product.)

The idea of optimal grids is to choose an f_k which is a good rational approximation to f on the spectral domain of interest, and to use the grid which yields the desired f_k. The impedance $f(\lambda)$ is a Stieltjes function of λ, and so we can use the well developed theory of rational approximations to Stieltjes functions [5]. That is, $f(\lambda)$ can be written as

$$(2.10) \qquad\qquad \int_{-\infty}^{0} (\lambda - \gamma)^{-1} d\sigma(\gamma)$$

for $\sigma(\lambda)$ some positive measure on $(-\infty, 0]$; the spectral measure. For finite L, the spectral measure is discrete. For elliptic problems, the spectral interval of interest, $[\lambda_1, \lambda_2]$ is to the right of the origin (away from the poles), and so f_k is chosen to be a near optimal Padé-Chebyshev approximation. For semi-infinite intervals ($L = \infty$), we will have a continuous spectral measure, and in this case we use either Padé-Chebyshev or optimal Zolotarev's approximation. The Padé-Chebyshev approximations will have exponential convergence in k;

$$(2.11) \qquad\qquad |f_k(\lambda) - f(\lambda)| \leq C e^{-4k/\sqrt[6]{\kappa}}$$

where $\kappa = \lambda_2/\lambda_1$. For Zolotarev's approximations, the convergence rate will depend logarithmically on κ [14]. For the discrete measure (finite L) case, the convergence will in fact be superexponential [5].

For wave problems, the spectral interval will contain some poles, and one can choose the rational approximation to f by combining Padé-Chebyshev approximations with pole-matching, as in [3], where the high order convergence was maintained. We discuss the applications to isotropic elliptic and wave problems in more detail below.

Once a suitable f_k is chosen, the corresponding grid can be constructed by solving an inverse spectral problem [8]. Then the convergence at $x = 0$ of the resulting numerical solution is exactly that of the rational approximation. Furthermore, the primary and dual grids associated with f_k can be reversed and used to approximate the solution to the Neumann problem

$$(2.12) \qquad\qquad \begin{aligned} \lambda u - u_{xx} &= 0 \\ -u_x(0) &= \alpha \\ u_x(L) &= 0. \end{aligned}$$

and exponential convergence is maintained [9]. We will refer to the continuous and discrete NtD maps corresponding to this Neumann problem as $f^N(\lambda)$ and $f_k^N(\lambda)$, respectively.

Throughout the paper we assume we have such a system of primary and dual grids which yield exponential convergence in our spectral interval of interest for problems (2.1) and (2.12). What we do here is describe how to apply these *same* grids to anisotropic problems, and investigate the convergence. To study the anisotropic convergence, we need to view $f_k(z)$ as a rational approximation to $f(z)$ for $z \in \mathbb{C}$, not just on the real line.

Before analyzing anisotropy we show how optimal grids work for isotropic elliptic and hyperbolic equations.

2.2. Elliptic equations. Consider, for example, the following boundary value problem for Laplace's equation on the rectangle $(0, L) \times (0, \tilde{L})$:

$$(2.13) \qquad -w_{xx} - w_{yy} = 0, \quad -w_x(0, y) = \phi(y), \quad w(L, y) = 0, \quad w \; \tilde{L}\text{-periodic in } y.$$

Let us assume that the data has bounded spectrum, that is,

$$(2.14) \qquad \varphi(y) = \sum_{j=-m}^{m} a_j e^{i\omega_j y},$$

where $\omega_j = 2j\pi/\tilde{L}$. Then by using the Fourier method, we can obtain the Dirichlet data exactly:

$$w(0, y) = \sum_{j=-m}^{m} f(\omega_j^2) a_j e^{i\omega_j y}$$

where f is the impedance function (2.6). We introduce a semidiscretization of (2.13) on a system of primary and dual lines given, respectively, by $x = x_j$ and $x = \hat{x}_j$, and consider a solution $\{W_j(y)\}_{j=1,\ldots,k}$ to

$$(2.15) \qquad -\hat{d}dW - W_{yy} = 0,$$

$$-(dW)|_0(y) = \varphi, \quad W_{k+1}(y) = 0, \quad W_j(y) \; \tilde{L}\text{-periodic in } y, \quad j = 1, \ldots k.$$

We can again apply the Fourier method to (2.15) to obtain

$$W_1(y) = \sum_{j=-m}^{m} f_k(\omega_j^2) a_j e^{i\omega_j y}.$$

So, we can bound the error of the Dirichlet data

$$
\frac{\|w(0, y) - W_1(y)\|_{L^2[0,\tilde{L}]}}{\|\varphi\|_{L^2[0,\tilde{L}]}} = \frac{\left\| \sum_{j=-m}^{m} a_j e^{i\omega_j y} (f - f_k)(\omega_j^2) \right\|_{L^2[0,\tilde{L}]}}{\left\| \sum_{j=-m}^{m} a_j e^{i\omega_j y} \right\|_{L^2[0,\tilde{L}]}}
$$

$$
= \frac{\sqrt{\sum_{j=-m}^{m} a_j^2 \left[(f - f_k)(\omega_j^2) \right]^2}}{\sqrt{\sum_{j=-m}^{m} a_j^2}}
$$

$$(2.16) \qquad \qquad \leq \max_{\lambda \in [\omega_1^2, \omega_m^2]} |f(\lambda) - f_k(\lambda)|.$$

Hence for a semi-discretized elliptic problem, if the grid were chosen by a near optimal rational approximation, the convergence will be exponential (2.11) on the line $x = 0$. Note that (2.14) was assumed only for simplicity of explanation; for example, we could have used any smooth φ (with fast enough decaying Fourier representation) and still obtained exponential convergence.

Also, we could have used different boundary conditions, or an arbitrary positive-definite finite-difference operator in y with spectral interval $[\omega_1^2, \omega_m^2]$ instead of $-w_{yy}$ in (2.13), in which case (2.16) would give the estimate for the x-discretization error only.

2.3. Hyperbolic equations. Let us consider the initial value problem for the one-dimensional wave equation on $[0, L] \times [0, T]$,

$$(2.17) \quad w_{xx} - w_{tt} = 0, \quad -w_x(0, t) = \varphi(t), \quad w(L, t) = 0, \quad w(x, 0) = 0, \quad w_t(x, 0) = 0,$$

where

$$\varphi(t) = \sum_{l=-n}^{n} b_l e^{i\eta_l t}$$

and $\eta_l = 2l\pi/T$. We assume T/L irrational to avoid resonances. With the help of the Fourier method we obtain

$$w(0, t) = \sum_{l=-n}^{n} b_l f(-\eta_l^2) e^{i\eta_l t}$$

where again f is the one dimensional impedance (2.6). We introduce a semidiscretization of (2.17) by the method of lines using $x = x_j$ and $x = \hat{x}_j$, and consider a solution $\{W_j(t)\}_{j=1,\ldots,k}$ to the approximate problem

$$W_{tt} - \hat{d}dW = 0,$$

$$-(dW)_0(t) = \varphi(t), \quad W_{k+1}(t) = 0, \; W_j(0) = 0, \quad \frac{dW_j}{dt}(0) = 0, \quad j = 1, \ldots, k.$$

Again using the Fourier method we obtain

$$W_1(t) = \sum_{l=-n}^{n} b_l f_k(-\eta_l^2) e^{i\eta_l t}.$$

Then the error bound for the Dirichlet data can be obtained as in the elliptic problem:

$$\frac{\|w(0, t) - W_1(t)\|_{L^2[0,T]}}{\|\varphi\|_{L^2[0,T]}} \leq \max_{\lambda \in [-\eta_n^2, 0]} |f(\lambda) - f_k(\lambda)|.$$

REMARK 2.1. An important difference between this problem and the elliptic one is that there are poles of f in the spectral interval due to the negativity of its lower bound. These poles are matched in the rational approximation. Hence we need to set k in (2.9), i.e., the number of terms in the rational approximation, to be at least equal to the number of these poles in the interval $[-\eta_n^2, 0]$. One can calculate that this is the integer part of $\frac{L\eta_n}{\pi} + 1/2$, which is approximately twice the number of wavelengths corresponding to the temporal frequency η_n within $[0, L]$. So, we arrive at the important conclusion that the exponential convergence

occurs when the average grid density exceeds two points per wave length, i.e., the Nyquist limit frequency. The convergence bound from [8] gives at least a logarithmic convergence rate proportional to $\sqrt[6]{\frac{\eta_n^2}{d}}$, where d is the distance between η_n^2 and the closest non-excluded pole of f. It shows that, asymptotically (for high frequencies), an appropriately chosen optimal grid finite difference scheme requires only two grid points per wavelength to converge.

Let us also consider a multidimensional hyperbolic equation, say in $[0, L] \times [0, \tilde{L}] \times [0, T]$,

$$w_{tt} - w_{yy} - w_{xx} = 0,$$
$$w_x(0, y, t) = -\varphi(y, t), \quad w(L, y, t) = 0,$$
$$w(x, y, 0) = 0, \quad w_t(x, y, 0) = 0,$$
$$w \quad \tilde{L}\text{-periodic in} \quad y$$

with data given by a finite sum of the form

$$\varphi = \sum_{j=-m}^{m} \sum_{l=-n}^{n} a_{jl} e^{i\eta_l t} e^{i\omega_j y},$$

with $\eta_l = \frac{2l\pi}{T}$ and $\omega_j = \frac{2j\pi}{\tilde{L}}$. Then we can calculate that the resulting Dirichlet data is given by

$$w(0, y, t) = \sum_{j,l} a_{jl} f\left(\omega_j^2 - \eta_l^2\right) e^{i(\eta_l t + \omega_j y)}.$$

We can use the semidiscretization

$$W_{tt} - W_{yy} - \hat{d}dW = 0$$

with appropriate initial and boundary conditions, and for the semidiscrete solution obtain

$$W_1(y, t) = \sum_{j,l} a_{jl} f_k\left(\omega_j^2 - \eta_l^2\right) e^{i(\eta_l t + \omega_j y)}.$$

Again, when the average grid density exceeds two points per wave length, the maximal possible spectral error

$$\frac{\|w(0, y, t) - W_1(y, t)\|_{L^2[0, \tilde{L}] \times [0, T]}}{\|\varphi\|_{L^2[0, \tilde{L}] \times [0, T]}} \leq \max_{\lambda \in [-\eta_n^2, \omega_m^2]} |f(\lambda) - f_k(\lambda)|$$

starts to decrease exponentially. The most difficult and the most important for the finite-difference approximation of wave problems are the propagative modes, that is, those with purely imaginary exponents. If we look at the solution in the entire domain,

$$w = \sum_{j,l} a_{jl} e^{i\left(\sqrt{\eta_l^2 - \omega_j^2} x + \eta_l y + \omega_j t\right)},$$

we see that these propagative modes correspond to $\eta_l^2 > \omega_j^2$. If one omits the so-called evanescent modes with real exponential decay in the x direction from the estimate, we have

$$\frac{\|w(0, y, t) - W_1(y, t)\|_{L^2[0, \tilde{L}] \times [0, T]}}{\|\varphi\|_{L^2[0, \tilde{L}] \times [0, T]}} \leq \max_{\lambda \in [-\eta_n^2, 0]} |f(\lambda) - f_k(\lambda)|.$$

One can similarly construct an exponentially convergent scheme for parabolic problems.

3. Anisotropy.

3.1. Motivation.
To motivate the material in the following sections, let us consider the constant coefficient anisotropic elliptic equation

$$(3.1) \qquad -v_{yy} + 2av_{xy} - v_{xx} = 0,$$

on the rectangle $(0, L) \times (0, \tilde{L})$, with periodic boundary conditions in y and Neumann data on the left and right sides. Assume that a is real and $|a| < 1$. This equation on a rectangle can be viewed as the Laplace equation on a parallelogram with bottom parallel to the x-axis and angle ϕ between its bottom and left sides. That is, if we make the change of variables

$$\begin{pmatrix} \tilde{x} \\ \tilde{y} \end{pmatrix} = \begin{pmatrix} 1 & 0 \\ \cos\phi & \sin\phi \end{pmatrix} \begin{pmatrix} x \\ y \end{pmatrix}$$

we obtain the equation (3.1) where $a = \cos\phi$. We consider the equation (3.1) in such a form for simplicity; it can be transformed to the more general anisotropic equation

$$-a_{11}v_{yy} + 2a_{12}v_{xy} - a_{22}v_{xx} = 0$$

by stretching along main coordinate axes without affecting exponential convergence of optimal grids. It is the mixed derivative term that needs special treatment.

Suppose we compute the Fourier coefficients in y of a solution to (3.1),

$$u_j(x) = \int_0^{\tilde{L}} v(x, y)e^{i\omega_j y}dy.$$

We have then that $u_j(x)$ satisfies the following equation in x,

$$(3.2) \qquad \omega_j^2 u_j - i2a\omega_j(u_j)_x - (u_j)_{xx} = 0.$$

For simplicity of exposition we will consider $\omega_j > 0$, as the analysis for $\omega_j < 0$ works in the same way. So, we will consider solutions to

$$(3.3) \qquad \lambda u - i2a\sqrt{\lambda}u_x - u_{xx} = 0,$$

and refer to this as our one dimensional anisotropic equation. When $a = 0$ and $\phi = \frac{\pi}{2}$, this corresponds to an isotropic problem. In this case, (3.3) has the two linearly independent solutions:

$$u = e^{\pm\sqrt{\lambda}x}.$$

For nontrivial a, we can represent solutions in the form

$$u = e^{b\sqrt{\lambda}x}$$

where complex b satisfies the quadratic equation

$$(3.4) \qquad b^2 + i2ab - 1 = 0.$$

That is,

$$b = -ia \pm \sqrt{-a^2 + 1} = -ie^{\pm i\phi}$$

where

$$\phi = \arccos a \in (0, \pi).$$

We will use b_1 and b_2 to denote the roots with negative and positive real parts, respectively. Note that it is not obvious how to apply optimal grids to (3.2). Since the grid is a staggered one, the first order term u_x lives on the grid dual to the one for u and u_{xx}. Therefore, applying the grids and differences (2.3) and (2.4) directly does not make geometric sense. In the sections that follow, we resolve this problem by rewriting the equation as a system. The techniques for the infinite and finite intervals are somewhat different; so we examine each separately. Also, for wave problems we need to consider a slightly more general form for the equation (3.2), and we do that for a bounded interval.

3.2. Semi-infinite interval. Let us now consider the problem

$$(3.5) \qquad \lambda u - i2a\sqrt{\lambda}u_x - u_{xx} = 0.$$

on $[0, \infty)$ with boundary conditions

$$(3.6) \qquad -u_x(0) = 1, \qquad \lim_{x \to \infty} u = 0.$$

Due to the infinity condition we we will have a unique solution with $b = b_1$, the root of (3.4) with negative real part. One can calculate that the NtD map (or impedance) is

$$(3.7) \qquad f^a(\lambda) := u(0) = -\frac{1}{b_1\sqrt{\lambda}} = f(b_1^2\lambda)$$

where f is the isotropic impedance (2.7). To apply optimal grids to this problem, we reformulate the equation as a second order system.

LEMMA 3.1. *The system*

$$(3.8) \qquad \begin{aligned} \lambda u - i2a\sqrt{\lambda}w_x - u_{xx} = 0 \\ \lambda w - i2a\sqrt{\lambda}u_x - w_{xx} = 0 \end{aligned}$$

on $[0, \infty)$ with boundary conditions

$$(3.9) \qquad \begin{aligned} -u_x(0) = 1, \qquad \lim_{x \to \infty} u = 0 \\ -w_x(0) = 1, \qquad \lim_{x \to \infty} w_x = 0 \end{aligned}$$

is equivalent to the problem (3.5) with boundary conditions (3.6).

Proof. Clearly, the solution u of (3.5), (3.6) satisfies (3.8), (3.9) with

$$w = u = -\frac{e^{b_1\sqrt{\lambda}x}}{b_1\sqrt{\lambda}}.$$

Furthermore, one can check that there are four linearly independent solutions of (3.8) which are solutions of the first order systems

$$(3.10) \qquad b\sqrt{\lambda}u = w_x, \qquad b\sqrt{\lambda}w = u_x,$$

with both roots b_i of (3.4):

$$\begin{pmatrix} e^{b_1\sqrt{\lambda}x} \\ e^{b_1\sqrt{\lambda}x} \end{pmatrix}, \begin{pmatrix} e^{-b_1\sqrt{\lambda}x} \\ -e^{-b_1\sqrt{\lambda}x} \end{pmatrix}, \begin{pmatrix} e^{b_2\sqrt{\lambda}x} \\ e^{b_2\sqrt{\lambda}x} \end{pmatrix}, \begin{pmatrix} e^{-b_2\sqrt{\lambda}x} \\ -e^{-b_2\sqrt{\lambda}x} \end{pmatrix}.$$

If we now impose the boundary conditions (3.9), the unique solution is

$$u = w = -\frac{e^{b_1 \sqrt{\lambda} x}}{b_1 \sqrt{\lambda}}$$

from which the result follows.   □

What we will do is apply the optimal grids directly on the problem (3.8), using the primary grid for u and the dual for w, to get the finite difference system

$$\lambda U_j - i 2a \sqrt{\lambda} \frac{W_j - W_{j-1}}{\hat{h}_j} - \frac{1}{\hat{h}_j} \left[\frac{U_{j+1} - U_j}{h_j} - \frac{U_j - U_{j-1}}{h_{j-1}} \right] = 0,$$

$$\lambda W_j - i 2a \sqrt{\lambda} \frac{U_{j+1} - U_j}{h_j} - \frac{1}{h_j} \left[\frac{W_{j+1} - W_j}{\hat{h}_{j+1}} - \frac{W_j - W_{j-1}}{\hat{h}_j} \right] = 0,$$

(3.11) $j = 1, \ldots, k$

with the discrete boundary conditions

(3.12) $\frac{U_1 - U_0}{h_0} = -1, \; U_{k+1} = 0, \qquad \frac{W_1 - W_0}{\hat{h}_1} = -1, \; \frac{W_{k+1} - W_k}{\hat{h}_{k+1}} = 0.$

We define the finite difference impedance by the average,

$$f_k^a(\lambda) = \frac{U_1 + W_0}{2},$$

and estimate how accurately it approximates $f^a(\lambda)$. What the following result shows is that the convergence of the anisotropic impedance depends on the convergence of the corresponding isotropic impedance on a ray in the complex plane.

PROPOSITION 3.2. *Let*

$$f_k^a(\lambda) = \frac{U_1 + W_0}{2}$$

be the numerical impedance computed from the system (3.11), (3.12) and let $f^a(\lambda)$ be the continuous impedance (3.7). Then the relative error of the impedance satisfies

$$\left| \frac{f_k^a(\lambda)}{f^a(\lambda)} - 1 \right| \leq C \left| \frac{f_k(b_1^2 \lambda)}{f(b_1^2 \lambda)} - 1 \right|^2$$

where b_1 is the root of (3.4) with negative real part, $f_k(z), f(z)$ are the discrete and continuous isotropic impedances (2.8), (2.7), and C is independent of k. That is, the error for the anisotropic impedance for real λ is on the order of the square of the isotropic impedance error on the ray in the complex plane

$$-e^{-i2\phi} \lambda$$

where $\phi = \arccos a, \, 0 < \phi < \pi$.

Proof. Consider the finite difference counterpart of (3.10),

(3.13) $b\sqrt{\lambda} \dot{U}_j = \frac{\dot{W}_j - \dot{W}_{j-1}}{\hat{h}_j}$

$$b\sqrt{\lambda} \, \dot{W}_j = \frac{\dot{U}_{j+1} - \dot{U}_j}{h_j},$$

$$j = 1, \ldots, k.$$

We will show that similar to in the continuous case, using both roots b_1 and b_2 of (3.4) in (3.13) gives a basis for all the solutions of (3.11). To see this, consider a solution $(\dot{U}, \dot{W})$ of (3.13). Eliminating $\dot{W}$ we obtain

$$(3.14) \qquad b^2 \lambda \dot{U}_j - \frac{1}{\hat{h}_j} \left[\frac{\dot{U}_{j+1} - \dot{U}_j}{h_j} - \frac{\dot{U}_j - \dot{U}_{j-1}}{h_{j-1}} \right] = 0.$$

With the help of (3.4), this equation becomes

$$(3.15) \qquad \lambda \dot{U}_j - i2ab\lambda \dot{U}_j - \frac{1}{\hat{h}_j} \left[\frac{\dot{U}_{j+1} - \dot{U}_j}{h_j} - \frac{\dot{U}_j - \dot{U}_{j-1}}{h_{j-1}} \right] = 0.$$

By then substituting the first equation of (3.13) into the second term of the left hand side of (3.15) we obtain the first equation of (3.11). Similarly, eliminating $\dot{U}$ from (3.13) we obtain

$$(3.16) \qquad b^2 \lambda \dot{W}_j - \frac{1}{h_j} \left[\frac{\dot{W}_{j+1} - \dot{W}_j}{\hat{h}_{j+1}} - \frac{\dot{W}_j - \dot{W}_{j-1}}{\hat{h}_j} \right] = 0,$$

and we can again show that it can be transformed to the second equation of (3.11). Hence we see that all solutions of (3.13) satisfy (3.11). For each b_i, the system (3.13) has two linearly independent solutions. Using both the roots we obtain a total of four linearly independent solutions to (3.11).

REMARK 3.3. Clearly the system (3.14), (3.16) is not equivalent to (3.11); the former also contains four more linearly independent solutions.

To estimate the convergence of f_k^a to f^a, we decompose the solution (U, W) of (3.11) into two linearly independent solutions $(\dot{U}^i, \dot{W}^i)$ of (3.13). These solutions are obtained by setting $b = b_i$, $i = 1, 2$ and imposing that the boundary conditions hold at infinity for $\dot{U}^i$:

$$(3.17) \qquad \dot{U}_{k+1}^i = 0.$$

From this condition and equation (3.14) we have

$$\dot{U}_1^i = f_k(b_i^2 \lambda) \frac{\dot{U}_1^i - \dot{U}_0^i}{h_0},$$

where f_k is the standard discrete isotropic impedance on the primary grid. Define the ratio

$$\delta_k(z) = \frac{f_k(z)}{f(z)}$$

and rewrite the impedance as

$$f_k(b^2 \lambda) = \frac{\delta_k(b^2 \lambda)}{\sqrt{b^2 \lambda}}.$$

By the representation (2.10), one can see that Stieltjes functions of complex conjugate arguments are also conjugate. The same holds for the discrete impedance by the formula (2.9). So, since

$$b_1^2 = \bar{b}_2^2,$$

we have that

$$(3.18) \qquad \delta_k(b_1^2 \lambda) = \bar{\delta}_k(b_2^2 \lambda).$$

Note that system (3.13) in general gives dual relationships between its solutions $\dot{U}$ and $\dot{W}$. If $\dot{U}$ satisfies (3.17), then from (3.13) we obtain

$$\frac{\dot{W}_{k+1} - \dot{W}_k}{\hat{h}_{k+1}} = 0$$

and

$$(3.19) \qquad \frac{\frac{\dot{W}_1 - \dot{W}_0}{\hat{h}_1}}{\dot{W}_0} = \frac{b^2 \lambda \dot{U}_1}{\frac{\dot{U}_1 - \dot{U}_0}{h_0}} = \frac{b^2 \lambda \delta_k(b^2\lambda)}{\sqrt{b^2\lambda}}.$$

If we consider (3.13) with boundary conditions (3.17) and

$$(3.20) \qquad \frac{\dot{U}_1 - \dot{U}_0}{h_0} = -1,$$

then from the second equation of (3.13)

$$\dot{W}_0 = -\frac{1}{b\sqrt{\lambda}},$$

and from (3.19) we obtain

$$(3.21) \qquad \frac{\dot{W}_1 - \dot{W}_0}{\hat{h}_1} = -\frac{b^2 \lambda \delta_k(b^2\lambda)}{b\sqrt{\lambda}\sqrt{b^2\lambda}} = -\text{sign}(\Re(b))\delta_k(b^2\lambda).$$

From here on we use $\dot{U}^i, \dot{W}^i$ to denote the solutions of (3.13), (3.17), (3.20) with $b = b_i$. Then U, W satisfying (3.11), (3.12) can be represented as

$$U = c_1 \dot{U}^1 + c_2 \dot{U}^2, \qquad W = c_1 \dot{W}^1 + c_2 \dot{W}^2,$$

where the c_i are determined by the boundary conditions (3.12) at the left. For brevity we define

$$\delta = \delta_k(b_1^2\lambda).$$

Then, using (3.20), (3.21) and (3.18), we obtain

$$c_1 = \frac{\bar{\delta} + 1}{2\Re(\delta)}, \qquad c_2 = \frac{\delta - 1}{2\Re(\delta)}.$$

This gives the discrete impedance

$$(3.22) \qquad f_k^a(\lambda) = \frac{(U_1 + W_0)}{2}$$
$$= \frac{(\bar{\delta} + 1)\dot{U}_1^1 + (\delta - 1)\dot{U}_1^2 + (\bar{\delta} + 1)\dot{W}_0^1 + (\delta - 1)\dot{W}_0^2}{4\Re(\delta)}.$$

We know that

$$\dot{U}_1^1 = -\frac{\delta}{b_1\sqrt{\lambda}}, \quad \dot{U}_1^2 = \frac{\bar{\delta}}{b_2\sqrt{\lambda}},$$

and

$$\dot{W}_0^i = -\frac{1}{b_i\sqrt{\lambda}}.$$

Substituting these into (3.22) we obtain

$$f_k^a(\lambda) = -\frac{1}{b_1\sqrt{\lambda}}\Delta,$$

where

$$\Delta = \frac{(\bar{\delta}+1)\delta - (\delta-1)\bar{\delta}\frac{b_1}{b_2} + (\bar{\delta}+1) + (\delta-1)\frac{b_1}{b_2}}{4\Re(\delta)}$$

$$= 1 + \frac{(1 - \frac{b_1}{b_2})(\delta-1)(\bar{\delta}-1)}{4\Re(\delta)}.$$

Now, if we assume that $|\delta - 1|$ is small, then

$$|\Delta - 1| = O(|\delta - 1|^2),$$

or

$$|f_k^a/f^a - 1| = O(|\delta_k(b_1^2\lambda) - 1|^2)$$

which completes the proof. $\Box$

So, the relative error of the approximation of the continuous impedance is on the order of the square of the relative error of the isotropic impedance $f_k(b^2\lambda)$. That is, we reduced the problem to that of the approximation of a Stieltjes function on the line

$$-e^{i2\phi}\lambda$$

for a positive interval of λ with

$$0 < \phi < \pi.$$

The Padé-Chebyshev approximations, generated from data for f for z on the positive real line will yield exponential convergence on finite regions of $\mathbb{C}$ which are away from the negative real axis, where we have the poles of both f_k and f [5]. Hence it is a consequence of rational approximation theory [5] that standard optimal grids for the isotropic problem will produce exponential convergence for the problem (3.5). Note that when $\phi = \pi/2$ we will have the standard isotropic problem; in the limit case $\phi \to 0$ the approximation line approaches the poles.

3.3. Two-sided problem on a finite interval. When applying optimal grids on finite regions or for use in domain decomposition, it is crucial that we can solve the two sided problem with spectral convergence at both ends. In this section we consider a two-sided and slightly more general anisotropic equation

$$(3.23) \qquad\qquad c\lambda u - i2a\sqrt{\lambda}u_x - u_{xx} = 0,$$

$$-u_x(0) = \alpha, \qquad u_x(L) = \beta$$

where we view c as a parameter. (For wave problems we will need to allow c to vary.) One difficulty with the two-sided problem is that the NtD map is now a 2×2 matrix valued function of λ, mapping the two-point Neumann data to the Dirichlet data:

$$(3.24) \qquad \begin{pmatrix} u(0) \\ u(L) \end{pmatrix} = F(\lambda) \begin{pmatrix} \alpha \\ \beta \end{pmatrix}.$$

First we should point out that for $c = 1$ and positive λ, the operator of equation (3.23) with the homogenous Neumann boundary condition is Hermitian positive-definite, so F is defined for any $\lambda > 0$.

Note that as in the last section, the true solution to the equation (3.23) is of the form

$$u = k_1 e^{b_1 \sqrt{\lambda}(x - L/2)} + k_2 e^{b_2 \sqrt{\lambda}(x - L/2)}$$

where $b = b_1, b_2$ now satisfy

$$(3.25) \qquad b^2 + i2ab - c = 0.$$

Dividing this solution into its odd and even (about $x = L/2$) parts,

$$u = u^o + u^e,$$

and plugging into (3.23), we obtain the following coupled system:

$$(3.26) \qquad c\lambda u^o - i2a\sqrt{\lambda}u_x^e - u_{xx}^o = 0,$$

$$c\lambda u^e - i2a\sqrt{\lambda}u_x^o - u_{xx}^e = 0,$$

$$-u_x^o(0) = \frac{\alpha + \beta}{2}, \quad u^o(L/2) = 0, \quad -u_x^e(0) = \frac{\alpha - \beta}{2}, \quad u_x^e(L/2) = 0,$$

which has the solution

$$u^o = k_1 \sinh b_1 \sqrt{\lambda}(x - L/2) + k_2 \sinh b_2 \sqrt{\lambda}(x - L/2)$$

$$u^e = k_1 \cosh b_1 \sqrt{\lambda}(x - L/2) + k_2 \cosh b_2 \sqrt{\lambda}(x - L/2).$$

Note that the differential operator is the same as in (3.8), but on a finite interval with boundary conditions. Since the solutions do not decay at infinity, both of the roots b_1 and b_2 will appear in the solution. Let us therefore decompose the solution in terms of the functions $(u^o)^1$, $(u^o)^2$, $(u^e)^1$ and $(u^e)^2$ which satisfy

$$(3.27) \qquad b_i^2 \lambda (u^o)^i - (u^o)_{xx}^i = 0$$
$$-(u^o)_x^i(0) = 1, \qquad (u^o)^i(L/2) = 0$$

and

$$(3.28) \qquad b_i^2 \lambda (u^e)^i - (u^e)_{xx}^i = 0$$
$$-(u^e)_x^i(0) = 1, \qquad (u^e)_x^i(L/2) = 0.$$

We know that the problem (3.27) has the continuous impedance

$$f(b_i^2 \lambda) = \frac{\tanh(Lb_i\sqrt{\lambda}/2)}{b_i\sqrt{\lambda}}$$

and one can compute that the Neumann problem (3.28) has the impedance

$$f^N(b_i^2 \lambda) = \frac{\coth(Lb_i\sqrt{\lambda}/2)}{b_i\sqrt{\lambda}}$$
$$= \frac{1}{b_i^2 \lambda f(b_i^2 \lambda)}.$$

We can now rewrite the odd and even parts of the solution as

$$(3.29) \qquad u^o = c_1(u^o)^1 + c_2(u^o)^2$$

$$u^e = c_1 b_1 \sqrt{\lambda} f(b_1^2 \lambda)(u^e)^1 + c_2 b_2 \sqrt{\lambda} f(b_2^2 \lambda)(u^e)^2$$

where the boundary conditions imply that c_1, c_2 solve the system

$$(3.30) \qquad \begin{bmatrix} 1 & 1 \\ b_1\sqrt{\lambda}f(b_1^2\lambda) & b_2\sqrt{\lambda}f(b_2^2\lambda) \end{bmatrix} \begin{bmatrix} c_1 \\ c_2 \end{bmatrix} = \begin{bmatrix} \frac{\alpha+\beta}{2} \\ \frac{\alpha-\beta}{2} \end{bmatrix}.$$

Now consider the following numerical approximation. We use the primary $\{x_i\}$ and dual $\{\hat{x}_i\}$ grids, respectively, for the odd and even parts of the solution U^o and U^e on the interval $(0, L/2)$; and similar to (3.11) we compute the finite difference approximation to (3.26):

$$(3.31) \qquad c\lambda U^o - i2a\sqrt{\lambda}\hat{d}U^e - \hat{d}dU^o = 0$$
$$c\lambda U^e - i2a\sqrt{\lambda}dU^o - d\hat{d}U^e = 0$$
$$-(dU^o)_0 = \frac{\alpha+\beta}{2}, \quad -(\hat{d}U^e)_1 = \frac{\alpha-\beta}{2}, \quad (U^o)_{k+1} = 0, \quad (\hat{d}U^e)_{k+1} = 0.$$

We will show the convergence of this finite difference solution at the boundary will again depend on the convergence of the isotropic impedance, as in the case of a semi-infinite interval. For this we introduce the discrete NtD map, $F_k(\lambda)$, where

$$(3.32) \qquad \begin{pmatrix} (U^o)_1 + (U^e)_0 \\ -(U^o)_1 + (U^e)_0 \end{pmatrix} = F_k(\lambda) \begin{pmatrix} \alpha \\ \beta \end{pmatrix}.$$

The following lemma says that we have a decomposition of the discrete solution which is similar to the above decomposition of the continuous solution.

LEMMA 3.4. *The finite difference solution to (3.31) can be written as*

$$(3.33) \qquad U^o = C_1(U^o)^1 + C_2(U^o)^2$$
$$U^e = C_1 b_1 \sqrt{\lambda} f_k(b_1^2 \lambda)(U^e)^1 + C_2 b_2 \sqrt{\lambda} f_k(b_2^2 \lambda)(U^e)^2$$

where $\{(U^o)^i, (U^e)^i\}$ are the solutions to

$$(3.34) \qquad \lambda b_i^2(U^o)^i - \hat{d}d(U^o)^i = 0, \quad -(dU^o)_0^i = 1, \quad (U^o)_{k+1}^i = 0$$

and

$$(3.35) \qquad \lambda b_i^2(U^e)^i - d\hat{d}(U^e)^i = 0, \quad -(\hat{d}U^e)_1^i = 1, \quad (\hat{d}U^e)_{k+1}^i = 0;$$

C_1 and C_2 satisfy the system

$$(3.36) \qquad \begin{bmatrix} 1 & 1 \\ b_1\sqrt{\lambda}f_k(b_1^2\lambda) & b_2\sqrt{\lambda}f_k(b_2^2\lambda) \end{bmatrix} \begin{bmatrix} C_1 \\ C_2 \end{bmatrix} = \begin{bmatrix} \frac{\alpha+\beta}{2} \\ \frac{\alpha-\beta}{2} \end{bmatrix}$$

where $f_k(z)$ is the discrete isotropic impedance for a bounded interval (2.6).

Proof. Notice that (3.33) as it is written will clearly satisfy all the discrete boundary conditions thanks to (3.34), (3.35) and (3.36). We will now show it is a solution to the difference system (3.31). From the equation (3.34) for each $(U^o)^i$ and the fact that each b_i is a root of (3.25) we have

$$\hat{d}d(U^o)^i = \lambda b_i^2(U^o)^i = c\lambda(U^o)^i - \lambda iab_i(U^o)^i.$$

Plugging (3.33) into the first equation in (3.31) and using the above to cancel, we get

$$(3.37) \qquad \begin{aligned} &-ia\sqrt{\lambda}C_1 b_1\sqrt{\lambda}f_k(b_1^2\lambda)\hat{d}(U^e)^1 + C_1\lambda iab_1(U^o)^1 \\ &-ia\sqrt{\lambda}C_2 b_2\sqrt{\lambda}f_k(b_2^2\lambda)\hat{d}(U^e)^2 + C_2\lambda iab_2(U^o)^2. \end{aligned}$$

Recall the duality property of the odd and even optimal finite difference grids,

$$\hat{d}(U^e)^i = (U^o)^i\frac{1}{f_k(b_i^2\lambda)},$$

from which we get that the above expression (3.37) is zero. The second equation in (3.31) is also satisfied by (3.33). One may check by plugging in and using the duality relation

$$\hat{d}(U^o)^i = (U^e)^i\frac{1}{f_k^N(b_i^2\lambda)} = (U^e)^i b_i^2\lambda f_k(b_i^2\lambda). \quad \square$$

Notice that thanks to the lemma, the true and finite difference solutions both have analogous decompositions into component parts. From this we can calculate the NtD maps for both problems. The continuous boundary solution from (3.29) is

$$\begin{bmatrix} u^o(0) \\ u^e(0) \end{bmatrix} = \begin{bmatrix} f(b_1^2\lambda) & f(b_2^2\lambda) \\ b_1\sqrt{\lambda}f(b_1^2\lambda)f^N(b_1^2\lambda) & b_2\sqrt{\lambda}f(b_2^2\lambda)f^N(b_2^2\lambda) \end{bmatrix} \begin{bmatrix} c_1 \\ c_2 \end{bmatrix}.$$

Recall that

$$f(b_i^2\lambda)f^N(b_i^2\lambda) = \frac{1}{b_i^2\lambda}.$$

Inverting the system (3.30) for c_1 and c_2 we have that

(3.38)

$$\begin{bmatrix} u^o(0) \\ u^e(0) \end{bmatrix} = \frac{1}{b_2\sqrt{\lambda}f(b_2^2\lambda) - b_1\sqrt{\lambda}f(b_1^2\lambda)} \begin{bmatrix} (b_2 - b_1)\sqrt{\lambda}f(b_1^2\lambda)f(b_2^2\lambda) & f(b_2^2\lambda) - f(b_1^2\lambda) \\ \frac{b_2}{b_1}f(b_2^2\lambda) - \frac{b_1}{b_2}f(b_1^2\lambda) & \frac{1}{\sqrt{\lambda}}\left(\frac{1}{b_2} - \frac{1}{b_1}\right) \end{bmatrix} \begin{bmatrix} \frac{\alpha+\beta}{2} \\ \frac{\alpha-\beta}{2} \end{bmatrix}$$

so that the NtD map (3.24) is

$$F(\lambda) = \frac{1}{b_2\sqrt{\lambda}f(b_2^2\lambda) - b_1\sqrt{\lambda}f(b_1^2\lambda)}Q\begin{bmatrix} (b_2 - b_1)\sqrt{\lambda}f(b_1^2\lambda)f(b_2^2\lambda) & f(b_2^2\lambda) - f(b_1^2\lambda) \\ \frac{b_2}{b_1}f(b_2^2\lambda) - \frac{b_1}{b_2}f(b_1^2\lambda) & \frac{1}{\sqrt{\lambda}}\left(\frac{1}{b_2} - \frac{1}{b_1}\right) \end{bmatrix}P$$

where

$$P = \begin{bmatrix} 1/2 & 1/2 \\ 1/2 & -1/2 \end{bmatrix}, \quad Q = \begin{bmatrix} 1 & 1 \\ -1 & 1 \end{bmatrix}.$$

By the above lemma and essentially the same calculation, the two sided discrete impedance (3.32), F_k is exactly the same as F except that each occurrence of the continuous impedance f is replaced by the discrete impedance f_k. Using these facts we can simplify the above to get the following proposition.

PROPOSITION 3.5. *Let b_1 and b_2 be the two roots of (3.25). Then the NtD map (3.24) for (3.23) is given by*

(3.39)

$$F(\lambda) = \frac{1}{\sqrt{\lambda}\left(b_2 f(b_2^2 \lambda) - b_1 f(b_1^2 \lambda)\right)} Q \left[\begin{array}{cc} (b_2 - b_1)\sqrt{\lambda} f(b_1^2 \lambda) f(b_2^2 \lambda) & f(b_2^2 \lambda) - f(b_1^2 \lambda) \\ \frac{b_2}{b_1} f(b_2^2 \lambda) - \frac{b_1}{b_2} f(b_1^2 \lambda) & \frac{1}{\sqrt{\lambda}}\left(\frac{1}{b_2} - \frac{1}{b_1}\right) \end{array} \right] P$$

while the discrete counterpart (3.32) is given by

(3.40)

$$F_k(\lambda) = \frac{1}{\sqrt{\lambda}\left(b_2 f_k(b_2^2 \lambda) - b_1 f_k(b_1^2 \lambda)\right)} Q \left[\begin{array}{cc} (b_2 - b_1)\sqrt{\lambda} f_k(b_1^2 \lambda) f_k(b_2^2 \lambda) & f_k(b_2^2 \lambda) - f_k(b_1^2 \lambda) \\ \frac{b_2}{b_1} f_k(b_2^2 \lambda) - \frac{b_1}{b_2} f_k(b_1^2 \lambda) & \frac{1}{\sqrt{\lambda}}\left(\frac{1}{b_2} - \frac{1}{b_1}\right) \end{array} \right] P$$

for

$$P = \left[\begin{array}{cc} 1/2 & 1/2 \\ 1/2 & -1/2 \end{array} \right], \quad Q = \left[\begin{array}{cc} 1 & 1 \\ -1 & 1 \end{array} \right],$$

and f and f_k the respectively continuous and discrete isotropic impedances (2.6) and (2.9) for the interval $[0, L/2]$.

Note that when $c = 1$, as will be the case for elliptic problems, the roots b_1 and b_2 are negative conjugate and again we have that the roots are

$$-ie^{\pm i\phi}$$

for $\phi = \arccos a$. So, the convergence of the solution at the endpoints $x = 0$ and $x = L$ depends on the convergence of $f_k(z)$ to $f(z)$ on the two complex conjugate rays

$$z = -e^{\pm i2\phi}\lambda,$$

for a positive interval of λ. One can see easily from the Stieltjes forms (2.6) and (2.9) of f and f_k that,

$$f(-e^{i2\phi}\lambda) = \overline{f}(-e^{-i2\phi}\lambda)$$

and

$$f_k(-e^{i2\phi}\lambda) = \overline{f}_k(-e^{-i2\phi}\lambda).$$

Hence it suffices to consider the approximation on just one of the rays. Also, because F exists for any positive λ, then as follows from (3.38) the denominator in the expression for F must be also nonzero for any positive λ. Obviously, the same is true for F_k, and so we have the following:

COROLLARY 3.6. *When $c = 1$ and $\lambda > 0$,*

$$\|F(\lambda) - F_k(\lambda)\| = O\left(\left|f(-e^{i2\phi}\lambda) - f_k(-e^{i2\phi}\lambda)\right|\right)$$

uniformly for any $\lambda \geq \lambda_{min} > 0$ and $0 < \phi_{min} \leq \phi \leq \phi_{max} < \pi$.

3.4. Anisotropic elliptic equations. Now, let us, for example, consider the problem on $(0, L) \times (0, \tilde{L})$:

$$-w_{xx} + 2aw_{xy} - w_{yy} = 0, \quad -w_x(0, y) = \phi(y), \quad w_x(L, y) = 0, \quad w \; \tilde{L}\text{-periodic in } y.$$

As before, we assume that the data has bounded spectrum, that is,

$$\varphi(y) = \sum_{j=-m}^{m} a_j e^{i\omega_j y},$$

where $\omega_j = 2j\pi/\tilde{L}$. Then we can compute that the solution is

$$w(x, y) = \sum_{j=-m}^{m} a_j u_j(x) e^{i\omega_j y},$$

where $u_j(x)$ solves

$$\omega_j^2 u_j - i2a\omega_j(u_j)_x - (u_j)_{xx} = 0, \quad -u_j'(0) = 1, \quad u_j'(L) = 0.$$

From this we obtain

$$w(0, y) = \sum_j \begin{pmatrix} 1 & 0 \end{pmatrix} F(\omega_j^2) \begin{pmatrix} 1 \\ 0 \end{pmatrix} a_j e^{i\omega_j y}$$

and similarly

$$w(L, y) = \sum_j \begin{pmatrix} 0 & 1 \end{pmatrix} F(\omega_j^2) \begin{pmatrix} 1 \\ 0 \end{pmatrix} a_j e^{i\omega_j y}$$

where F is the two-sided impedance (3.39) with $c = 1$. We will solve this problem using the semi-discretization on the lines $x = x_j$ and $x = \hat{x}_j$ for the halved interval $(0, L/2)$.

$$-W_{yy}^o - 2a\hat{d}W^e - \hat{d}dW^o = 0, \qquad -W_{yy}^e - 2adW^o - d\hat{d}W^e = 0,$$

$$-(dW^o)_0(y) = \phi(y)/2, \quad W_{k+1}^o(y, t) = 0,$$

$$-\left(\hat{d}W^e\right)_1(y) = \phi(y)/2, \quad \left(\hat{d}W^e\right)_{k+1}(y, t) = 0,$$

$$W^o(y), \; W^e(y) \text{ are } \tilde{L} - \text{periodic in } y.$$

This semi-discrete problem then has solutions at $x = 0$ and $x = L$, respectively, given by

$$W_1^o(y) + W_0^e(y) = \sum_j \begin{pmatrix} 1 & 0 \end{pmatrix} F_k(\omega_j^2) \begin{pmatrix} 1 \\ 0 \end{pmatrix} a_j e^{i\omega_j y}$$

$$-W_1^o(y) + W_0^e(y) = \sum_j \begin{pmatrix} 0 & 1 \end{pmatrix} F_k(\omega_j^2) \begin{pmatrix} 1 \\ 0 \end{pmatrix} a_j e^{i\omega_j y}.$$

From these formulae and Corollary 3.6, the error from this x-discretization at both sides $x = 0$ and $x = L$ will be

$$O\left(\max_{\lambda \in [\omega_1^2, \omega_m^2]} |f(-e^{i2\phi}\lambda) - f_k(-e^{i2\phi}\lambda)|\right).$$

3.5. Anisotropic hyperbolic equations. Let us now consider a wave problem on in $[0, L] \times [0, \tilde{L}] \times [0, T]$,

$$
\begin{aligned}
w_{tt} - w_{yy} - 2aw_{xy} - w_{xx} &= 0, \\
w_x(0, y, t) = -\varphi(y, t), \quad w_x(L, y, t) &= 0, \\
w(x, y, 0) = 0, \quad w_t(x, y, 0) &= 0, \\
w \quad \tilde{L}\text{-periodic in} \quad y
\end{aligned}
$$

(3.41)

with data φ given by a finite sum of the form

$$
\varphi = \sum_{j,l} a_{jl} e^{i\eta_l t} e^{i\omega_j y}
$$

where, as before, $\eta_l = 2\pi l/T$ and $\omega_j = 2\pi j/\tilde{L}$ are the temporal and spatial frequencies, respectively. The solution to (3.41) can be expressed as

$$
w(x, y, t) = \sum_{j,l} a_{jl} u_{jl}(x) e^{i\eta_l t} e^{i\omega_j y},
$$

where the u_{jl} satisfy

$$
u_{jl}(\omega_j^2 - \eta_l^2) - 2ia\omega_j(u_{jl})_x - (u_{jl})_{xx},
$$

$$
-(u_{jl})_x(0) = 1, \quad (u_{jl})_x(L) = 0.
$$

This is exactly the two-sided problem (3.23) with

(3.42)
$$
c = \frac{\omega_j^2 - \eta_l^2}{\omega_j^2}.
$$

For the case $c < a^2$, which is our primary interest here, the problem become indefinite, i.e., it will have resonances. We need to assume, then, that η_l are not resonance frequencies. One can compute that a solution u_{jl} is some combination of

$$
e^{b_1 \omega_j x}, \quad e^{b_2 \omega_j x}
$$

where b_1, b_2 are the two roots of

$$
b^2 + i2ab - c.
$$

By the analysis of the previous section, the resulting Dirichlet data for w is given by

$$
w(0, y, t) = \sum_{j,l} \begin{pmatrix} 1 & 0 \end{pmatrix} F^{jl} \begin{pmatrix} 1 \\ 0 \end{pmatrix} a_{jl} e^{i\eta_l t} e^{i\omega_j y},
$$

where

$$
F^{jl} = F(\omega_j^2)
$$

is the two-sided impedance from (3.39), with c given by (3.42). For the semi-discretized problem, we again use the system of primary and dual lines $x = x_j$ and $x = \hat{x}_j$, and divide

the solution into its odd and even parts about $x = L/2$. We solve for $\{W_j^o(y,t)\}_{j=1,\ldots,k+1}$, $\{W_j^e(y,t)\}_{j=0,\ldots,k}$ on the primary and dual lines, respectively, which satisfy

(3.43)
$$W_{tt}^o - W_{yy}^o - 2a\hat{d}W_y^e - \hat{d}dW^o = 0,$$
$$W_{tt}^e - W_{yy}^e - 2adW_y^o - d\hat{d}W^e = 0,$$

$$W_j^o(y,0) = 0, \quad \frac{d}{dt}W_j^o(y,0) = 0, \quad j = 1,\ldots k+1,$$

$$W_j^e(y,0) = 0, \quad \frac{d}{dt}W_j^e(y,0) = 0, \quad j = 0,\ldots k,$$

$$-(dW^o)_0(y,t) = \phi(y,t)/2, \quad W_{k+1}^o(y,t) = 0,$$

$$-\left(\hat{d}W^e\right)_1(y,t) = \phi(y,t)/2, \quad \left(\hat{d}W^e\right)_{k+1}(y,t) = 0,$$

$$W^o(y,t),\ W^e(y,t) \text{ are } \tilde{L} - \text{periodic in } y.$$

Again using the Fourier method, the resulting semi-discretized Dirichlet data is then

$$W_1^o(y,t) + W_0^e(y,t) = \sum_{j,l} \begin{pmatrix} 1 & 0 \end{pmatrix} F_k^{jl} \begin{pmatrix} 1 \\ 0 \end{pmatrix} a_{jl} e^{i\eta_l t} e^{i\omega_j y},$$

where

$$F_k^{jl} = F_k(\omega_j^2)$$

is the two-sided discrete impedance from (3.40), where again c is given by (3.42). For $c < a^2$, matrix-valued function $F(\lambda)$ has poles, so we can not formulate an exact counterpart of Corollary 3.6. However, since we have assumed that the η_l are not resonance frequencies, all entries of $F(\omega_j^2)$ are bounded. Hence it follows from the equivalent representation (3.38) that the denominators of $F(\omega_j^2)$ are nonzero. In this case, one can see explicitly from these formulae that for large enough k the error of the Dirichlet data can be estimated as

$$\|F(\omega_j^2) - F_k(\omega_j^2)\| = O\left(\max_{i=1,2} |f(b_i^2\omega_j^2) - f_k(b_i^2\omega_j^2)|\right),$$

where b_i are the roots of

$$b^2 + i2ab - \frac{\omega_j^2 - \eta_l^2}{\omega_j^2}.$$

Note that

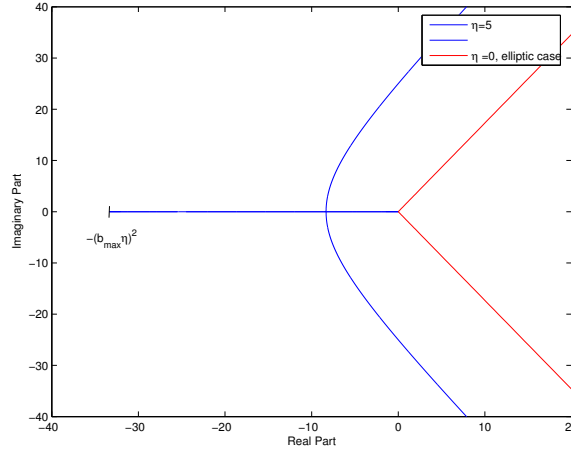$$b_1 = -ia + \sqrt{c - a^2}$$

$$b_2 = -ia - \sqrt{c - a^2}.$$

FIG. 3.1. *Spectral approximation curves in the complex plane for fixed temporal frequency η and varying spatial frequency ω. Here $a = \cos \phi = 0.5$.*

Consider now the modes which are propagative in x, that is, when $c < a^2$ and the roots b_1, b_2 are purely imaginary. This means that, just as in the isotropic wave problem of Section 2.3, we need f_k to be a good approximation to f on the negative real axis- exactly where f has poles. So, just as before, f_k needs to be defined by matching these poles.

We can further examine the negative real spectral interval that needs to be approximated by f_k by considering the following form of a propagative mode:

$$u = e^{i\eta_l(bn_x x + bn_y y + t)},$$

where $n = (n_x, n_y)$, $\|n\| = 1$, and $bn_y = \frac{\omega_j}{\eta_l}$. If we substitute this representation into the differential equation (3.41) we obtain

$$b = \langle An, n \rangle^{-1},$$

where A is the coefficient matrix of the elliptic part of the operator,

$$A = \begin{pmatrix} 1 & a \\ a & 1 \end{pmatrix}.$$

From this we see that $b \leq b_{max}$, where b_{max} is the reciprocal of the minimal eigenvalue of A. The latter is just the minimal wave speed for the anisotropic media. So, the error for the Dirichlet data corresponding to the propagative modes will depend on

$$\max_{z \in [-(\eta_n b_{max})^2, 0]} |f(z) - f_k(z)|.$$

We would therefore require the elimination of the poles on the interval $[-(\eta_n b_{max})^2, 0]$. This is similar to what was done for the isotropic problem on the smaller interval $[-\eta_n^2, 0]$ where the minimal wave speed was 1. Note that for a given η_n, the grid size should still be inversely proportional to the minimal wave speed, *i.e., it will require approximately the same number of grid points per wavelength as for the isotropic problem*. The evanescent spectrum is well separated from the spectrum of $\frac{d^2}{dx^2}$, so the semi-discretized finite difference solution will converge exponentially (with uniform exponential rate) with k on the line $x = 0$. In

Figure 3.1 we plot an example of $(b_i\omega)^2$ curves for a fixed η and varying ω. For $\eta = 5$, we see the two components of the spectrum in blue. The horizontal interval $[-(b_{max}\eta)^2, 0]$ corresponds to the propagative modes, and the curvilinear part corresponds to the evanescent modes. This is shown next to the corresponding red lines for the elliptic case, that is, when $\eta = 0$.

4. Numerical experiments. Optimal grids were successfully implemented (without mathematical foundation) to the 3D dissipative (elliptic) anisotropic Maxwell's equations in induction well logging applications for oil exploration [7]. The exponential convergence was experimentally observed for 3D anisotropic problems in unbounded domains.

Here we demonstrate the use of optimal grids for the two dimensional scalar wave equation with domain decomposition. In practice, we design optimal grids for constant coefficients, but, indeed, our objective is to apply them for variable coefficient problems. One way to do this is by decomposing the domain. Let us assume, for simplicity, that we solve a piecewise constant coefficient elliptic equation in $\Omega = \Omega_1 \cap \Omega_2$, such that in every subdomain we have the Laplace equation. If the NtD maps in every subdomain are approximated with accuracy ϵ, and the approximate solution satisfies the conjugation condition (continuity of the solution and normal component of the current) on the interface S between the subdomains, then the solution of the entire problem would be approximated with $O(\epsilon)$ error on S. This is why we can use the optimal grids, which were designed for constant coefficient problems, in the homogeneous subdomains of variable coefficient problems. By the same reasoning they are particularly useful in the exterior part of unbounded domains.

Now let us apply optimal grids to the problem

$$u_{tt} = u_{xx} + 2au_{xy} + u_{yy}.$$

We introduce a y-discretization with, respectively, primary and dual grids (see Figure 4.1):

$$\{y_i\}, \quad i = 0, 1, \ldots, m+1$$

and

$$\{\hat{y}_i\}, \quad i = 0, \ldots, k$$

in a similar manner as for the x-grid. This yields the semi-discrete system (3.43)

$$W_{tt}^o - \hat{d}_y d_y W^o - 2a\hat{d}\hat{d}_y W_y^e - \hat{d}dW^o = 0$$

(4.1)

$$W_{tt}^e - d_y \hat{d}_y W^e - 2ad\hat{d}_y W_y^o - d\hat{d}W^e = 0$$

where the FD operators d_y and $\hat{d}_y$ are the counterparts of d and $\hat{d}$, respectively. The obtained ODE system (4.1) is solved by the standard explicit time-stepping.

The convergence analysis of (3.43) can be extended to (4.1) in the following way. The error of (4.1) can be estimated as the error of (3.43) plus the error of the y-discretization. Following the approach of [4], we compute the rational approximation, not to the exact impedance, but to the impedance of a fine equidistant grid. Such grids are easier to compute and do not generate artificial reflections when combined with fine equidistant grids in multi-domain settings. The extremely fast convergence of the Padé-Chebyshev algorithm after the elimination of the resonance poles, i.e., after average grid density exceeds Nyquist limit of two points per wave length, allows us to obtain an accurate (with single precision accuracy) approximation of the fine-grid impedance on the prescribed spectral interval with very small cost. So, what we will do is compare the results for such spectrally "equivalent" coarse optimal and fine equidistant grids.

0   1

FIG. 4.1. *Sample optimal grid. Dots are the primary points and crosses are the dual grid points.*

In the first experiment we use a homogeneous, anisotropic medium given by a symmetric 2×2 matrix that has value 2 on the diagonal and 1 off the diagonal. The computations are done on a square centered about the origin with half side equal to one, and the source function is a Gaussian pulse with center frequency equal to 10 Hz. The source is located at the origin.

In this first experiment we perform the computations three times. The first is with an equidistant grid with 8 points per minimum wavelength (with the respect of the minimal wavespeed in the model). In the second computation, we use the equidistant grid on the left half while the right half of the domain we used an equivalent optimal grid in the x direction. The optimal grid in the right half plane has slightly less than 1/3 of the nodes of the equidistant grid. In the third computation, we used the optimal grid in both the x direction on the right half of the domain and in the y direction on the top half of the domain. The tensor product optimal grid in the upper right region of the domain has approximately 1/10 of the number of nodes on the grid as the equidistant mesh in the same region. This is a less significant savings than one would have if higher accuracy were needed. For comparison, if we were to need 16 points per wavelength, the savings would be about 34 times; for 32 points per wavelength the savings would be over 100 times. In Figure 4.2 we present a snapshot of the wave at the same time for the three different grids. The gridlines are also shown on the plots, but for convenience only every 10th gridline is drawn in each direction.

We see that the profiles present an ellipse, as expected for anisotropic media. On the first and equidistant grid, this ellipse has a well-defined, non-dispersive front. In the second picture of Figure 4.2, in the optimal grid region one sees the numerical dispersion caused by the coarsening of the grid steps. This dispersion, however, does not affect the accuracy on the left half of the domain. The optimal grid accurately reproduces the NtD map at $x = 0$, that is why the results in the left half plane are accurate. Similarly, in the third snapshot we observe that although there is large numerical dispersion in the coarse grid region, this error does not propagate into fine grid region. We note that while a rigorous approach to tensor product optimal grids goes beyond the analysis described here, it is not difficult to see why they may work. Using an equivalent optimal grid in y in the upper half plane leaves the NtD map of (4.1) (with fine y-grid) at $y = 0$ unchanged. This is why the results in the lower left quarter remain unchanged compared to the fine uniform y-grid in the second picture. In fact, the difference between the first and third pictures in the bottom left region is less than 0.1%, while the error between these computations, with 8 points per wavelength, and the true solution, is itself on the order of 1%.

For the second experiment, our geometry is a model of a simple vertical well, or borehole, with an anisotropic background medium. See Figure 4.3. The square of computation is the same, but the medium now varies in the x direction. For $x \in [-0.25, 0.25]$ the medium is an isotropic fluid with speed 1, but outside of this region we have an anisotropic solid represented by the 2×2 matrix with 2 on the diagonal and 1 on the off-diagonal. We first perform the computation using a fine equidistant grid. In the second computation, we use a fine equidistant grid within the isotropic borehole region and an optimal grid coarsening in the x direction in the outer, anisotropic, domain. Figure 4.4 shows the wave before it hits the anisotropic region. In both cases it is still within the fine gridded region. In Figure 4.5, we see the anisotropy influencing the wavefront and the beginning of numerical dispersion with
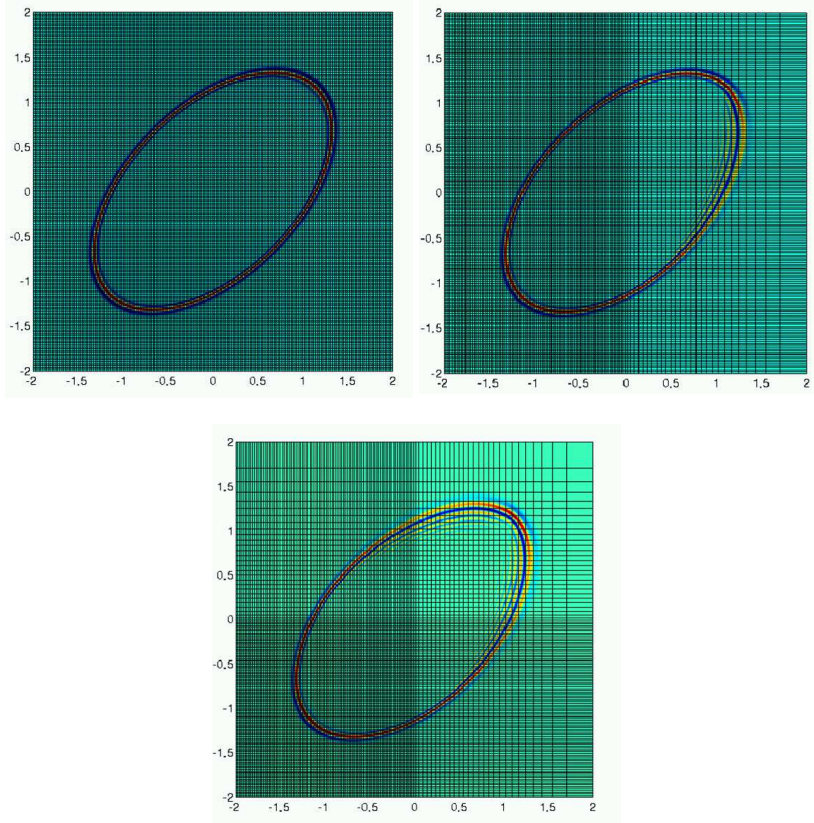
FIG. 4.2. *Wave in Homogeneous Anisotropic Media*

the coarse grid. Finally in Figure 4.6, we see that the grid coarsening and dispersion in the outer region has not affected the accuracy of the solution in the borehole region, where the receivers are located.

5. Discussion. In this manuscript, we have demonstrated that if one uses pre-existing optimal grids on the anisotropic problem (1.3) on a finite or semi-infinite interval by using the schemes described above, the convergence of the NtD map is on the order of the convergence of that of the isotropic NtD map on a ray in the complex plane. In particular, this says that if the grids were computed from a Padè-Chebyshev or Zolotarev's rational approximation, the convergence will be exponential. We also showed that for wave problems, the propagative modes require a spectral approximation on the negative real axis where the poles are located, similar to the isotropic case.

We also presented some qualitative numerical results for the two dimensional scalar wave equation in anisotropic media. We saw that the error in the coarsely gridded optimal grid subregions did not penetrate into the high accuracy regions, even if the two regions did not have the same material properties. This shows that the optimal grids, used in one or more directions, can greatly reduce the system size for a given accuracy at a receiver location.

As is the case for isotropic problems, optimal grids achieve spectral (generally exponential) convergence for the impedance response, or NtD map, of an interval, whether finite or semi-infinite. In other words, a coarse optimal grid will yield an approximation of this
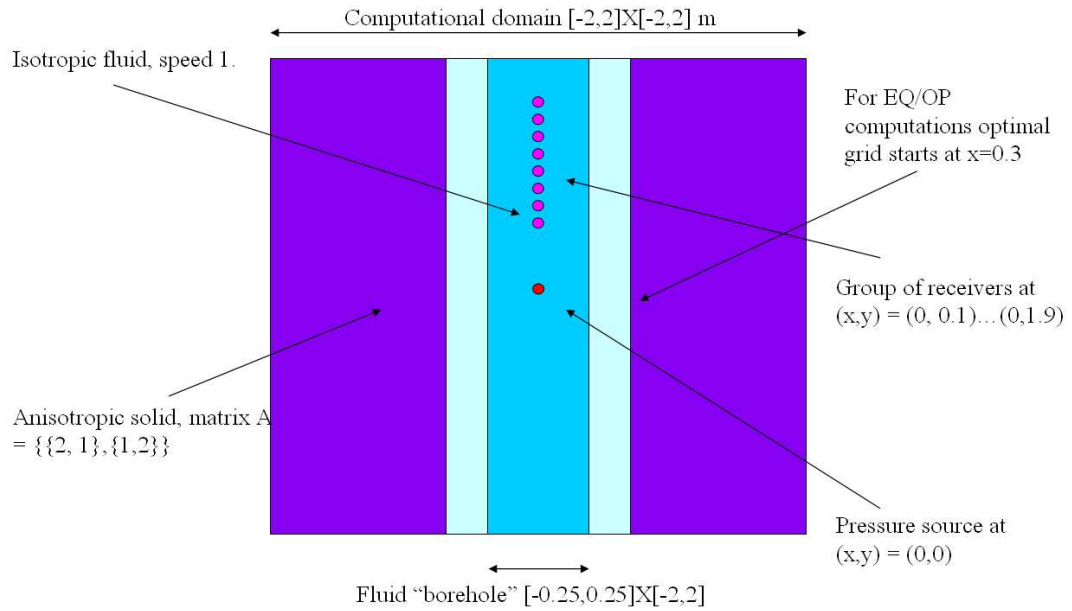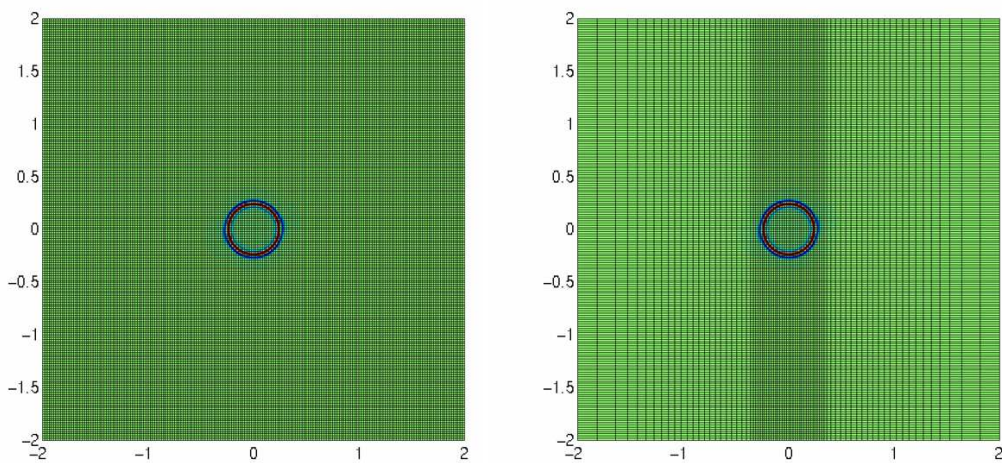
Acoustic logging problem

Computational domain [-2,2]X[-2,2] m

Isotropic fluid, speed 1.

For EQ/OP computations optimal grid starts at x=0.3

Group of receivers at (x,y) = (0, 0.1)...(0,1.9)

Anisotropic solid, matrix A = {{2, 1},{1,2}}

Pressure source at (x,y) = (0,0)

Fluid "borehole" [-0.25,0.25]X[-2,2]

FIG. 4.3. *Borehole Geometry*

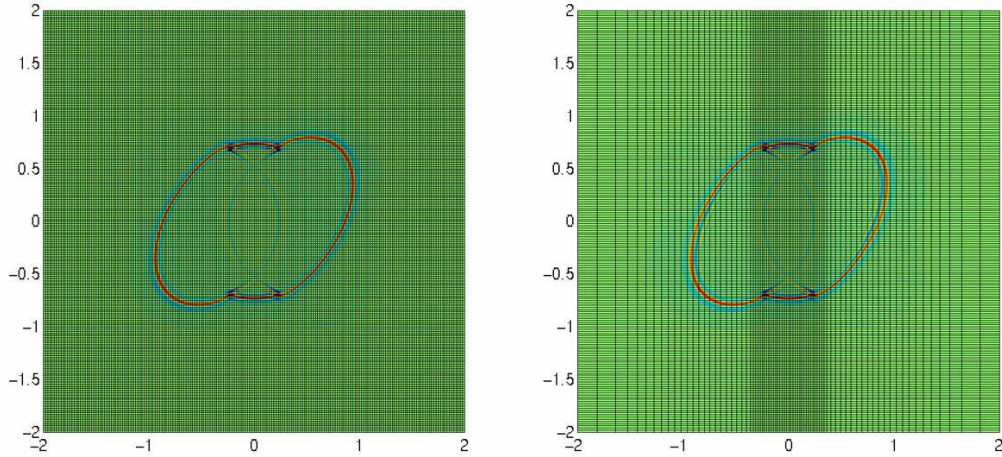FIG. 4.4. *Wave in Borehole Model: t=0.3*
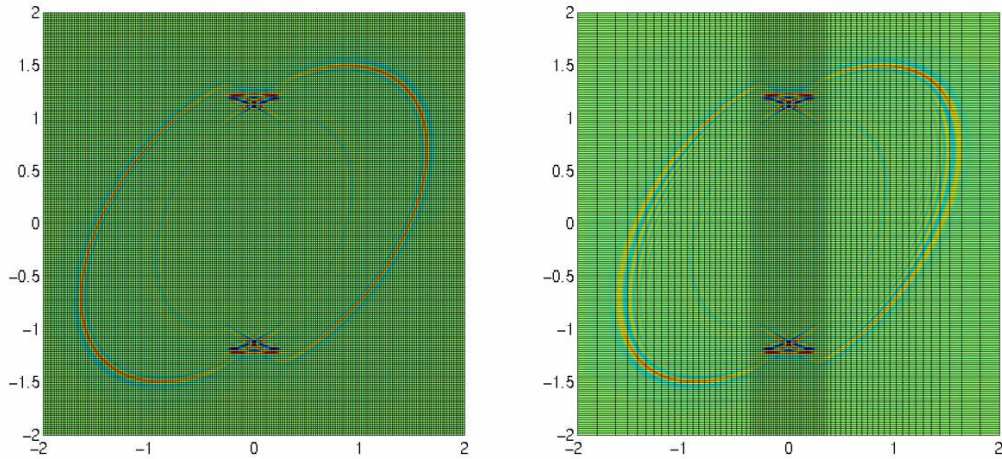
FIG. 4.5. *Wave in Borehole Model: t=0.8*

FIG. 4.6. *Wave in Borehole Model: t=1.3*

response equivalent to that of a very fine (exponentially finer) equidistant grid. Because it is the NtD map that completely determines the coupling of a domain with its neighbor(s), subdomains can be discretized very coarsely without affecting the accuracy of the solution in the finely gridded regions. Subregions are coupled using standard conjugation conditions. Furthermore, these subregions need not have the same material properties.

The next step will be to apply these techniques to more complex borehole geometries. This will require truly two dimensional domain decomposition, as was done for isotropic problems in [3]. To show that spectral convergence will be maintained for such problems, one needs to examine the convergence of the higher dimensional NtD map computed with tensor product optimal grids. We are currently working to show that the Galerkin equivalence described in [10] is maintained for the two dimensional NtD map in the sense of its representation in the eigenbases. What this will mean computationally is that we can use optimal

grids in both directions on rectangular, homogeneous, anisotropic subdomains (or geometries with parallelograms) while maintaining high order convergence. A rigorous analysis and numerical experiments will be provided in a forthcoming paper.

REFERENCES

[1] V. I. AGOSHKOW, *Poincaré-Steklov's operators and domain decomposition methods in finite dimensional spaces.*, in Domain Decomposition Methods for Partial Differential Equations I, R. Glowinski, et. al., eds., SIAM, Philadelphia, PA, 1988, pp. 73–112.

[2] S. ASVADUROV, V. DRUSKIN, M. N. GUDDATI, AND L. KNIZHNERMAN, *On optimal finite-difference approximation of PML.*, SIAM J. Numer. Anal., 41 (2003), pp. 287–305.

[3] S. ASVADUROV, V. DRUSKIN, L. KNIZHNERMAN, *Application of the difference Gaussian rules to the solution of hyperbolic problems.*, J. Comput. Phys., 158 (2000), pp. 116–135.

[4] S. ASVADUROV, V. DRUSKIN, L. KNIZHNERMAN, *Application of the difference Gaussian rules to the solution of hyperbolic problems. II. Global Expansion.*, J. Comput. Phys., 175 (2002), pp. 24–49.

[5] G. A. BAKER AND P. GRAVES-MORRIS, *Padé Approximants*, Addison-Wesley Publishing Co., London, 1996.

[6] L. BORCEA AND V. DRUSKIN, *Optimal finite difference grids for direct and inverse Sturm-Liouville problems.*, Inverse Problems, (2002), pp. 979–1001.

[7] S. DAVYDYCHEVA, V. DRUSKIN, AND T. M. HABASHY, *An efficient finite-difference scheme for electromagnetic logging in 3D anisotropic inhomogeneous media*, Geophysics, 68 (2003), pp. 1525–1536.

[8] V. DRUSKIN AND L. KNIZHNERMAN, *Gaussian spectral rules for three-point second differences. I. A two-point positive definite problem in a semi-infinite domain.*, SIAM J. Numer. Anal., 37 (2000), pp. 403–422.

[9] V. DRUSKIN AND L. KNIZHNERMAN, *Gaussian spectral rules for second order finite-difference schemes. Mathematical journey through analysis, matrix theory, and scientific computation.*, Numer. Algorithms, 25 (2000), pp. 139–159.

[10] V. DRUSKIN AND S. MOSKOW, *Three-point finite difference schemes, Padé and the spectral Galerkin method. I. One-sided impedance approximation.*, Math. Comp., 71 (2002), pp. 995–1019.

[11] B. ENGQUIST AND A. MAJDA, *Radiation boundary conditions for acoustic and elastic wave calculations*, Comm. Pure Appl. Math., 32 (1979), pp. 313–357.

[12] M. J. GANDER, F. MAGOULES, AND F. NATAF, *Optimized Schwarz methods without overlap for the Helmholtz equation.*, SIAM J. Sci. Comput., 24 (2002), pp. 38–60.

[13] D. GIVOLI, I. PATLASHENKO, AND J. B. KELLER, *DtN schemes for nonlinear problems in unbounded domains.* in Computational mechanics (Buenos Aires, 1998), CD-ROM file, Centro Internac. Mtodos Numr. Ing., Barcelona, 1998.

[14] D. INGERMAN, V. DRUSKIN, AND L. KNIZHNERMAN, *Optimal finite difference grids and rational approximation of the square root. I. Elliptic problems.*, Comm. Pure Appl. Math., 53 (2000), pp. 1039–1066.

[15] M. GUDDATI AND J. TASSOULAS *Continued-fraction absorbing boundary conditions for the wave equation*, J. Comp. Acoust., 8 (2000), pp. 139–156.

[16] V. I. LEBEDEV *Difference analogies of orthogonal decompositions of basic differential operators and some boundary value problems. I*, Soviet Comput. Math. Math. Physics., 4 (1964), pp. 449–465 (in Russian).

[17] S. MOSKOW, V. DRUSKIN, T. HABASHY, P. LEE, AND S. DAVYDYCHEVA, *A finite difference scheme for elliptic equations with rough coefficients using a Cartesian grid nonconforming to interfaces.*, SIAM J. Numer. Anal., 36 (1999), pp. 442–464.

[18] A. QUARTERONI AND A. VALLI, *Theory and application of Steklov-Poincaré operators for boundary value problems.*, in Applied and Industrial Mathematics, R. Spigler ed., Kluwer, Dordrecht, 1991, pp. 179–203.

[19] J. SYLVESTER AND G. UHLMANN *The Dirichlet to Neumann map and applications.*, in Inverse Problems in Partial Differential Equations, (Arcata, CA, 1989), SIAM, Philadelphia, PA, 1990, pp. 101–139.